CHEMICAL BIOLOGY

Restored iron transport by a small molecule promotes absorption and hemoglobinization in animals

Anthony S. Grillo,[1] Anna M. SantaMaria,[2] Martin D. Kafina,[3] Alexander G. Cioffi,[2] Nicholas C. Huston,[3] Murui Han,[4] Young Ah Seo,[5] Yvette Y. Yien,[3] Christopher Nardone,[2] Archita V. Menon,[4] James Fan,[1] Dillon C. Svoboda,[2] Jacob B. Anderson,[1] John D. Hong,[1] Bruno G. Nicolau,[1] Kiran Subedi,[1] Andrew A. Gewirth,[1] Marianne Wessling-Resnick,[6]* Jonghan Kim,[4]* Barry H. Paw,[3,7,8]* Martin D. Burke[1,2,9]*

Multiple human diseases ensue from a hereditary or acquired deficiency of iron-transporting protein function that diminishes transmembrane iron flux in distinct sites and directions. Because other iron-transport proteins remain active, labile iron gradients build up across the corresponding protein-deficient membranes. Here we report that a small-molecule natural product, hinokitiol, can harness such gradients to restore iron transport into, within, and/or out of cells. The same compound promotes gut iron absorption in DMT1-deficient rats and ferroportin-deficient mice, as well as hemoglobinization in DMT1- and mitoferrin-deficient zebrafish. These findings illuminate a general mechanistic framework for small molecule–mediated site- and direction-selective restoration of iron transport. They also suggest that small molecules that partially mimic the function of missing protein transporters of iron, and possibly other ions, may have potential in treating human diseases.

Site- and direction-selective transmembrane ion transport is achieved in most living systems through the concerted functions of active ion-transport proteins that generate localized electrochemical gradients and the passive ion-transport proteins that use them (*1*). Deficiencies of passive ion-transport proteins cause many human diseases, including anemias, cystic fibrosis, arrhythmias, and neurological, skeletal muscle, endocrine, and renal disorders (*2*–*5*). Because the corresponding active ion-transport proteins typically remain functional, there may be a buildup of ion gradients upstream of the membranes that normally host these missing proteins. Noting the capacity for these robust networks to achieve ion-selective transport despite the unselective nature of many ion-transport proteins (*1*, *2*), we hypothesized that small molecules capable of autonomously performing ion transport could leverage such gradients to restore transmembrane ion flux in a site- and direction-selective manner (Fig. 1A).

Iron homeostasis, in particular, is maintained by dynamic networks of active and passive iron-transport proteins and their regulators that permit essential use while minimizing toxicity of this redox-active metal (*2*). No known regulatory mechanisms of iron excretion exist (*6*), and systemic iron levels are thus primarily controlled through rigorous regulation of dietary iron absorption (*2*, *6*). Deficiencies or dysfunction of proteins involved in iron transport, homeostasis, or metabolism often impede the movement of iron into, within, and/or out of cells (Fig. 1A) and are associated with more than 25 Mendelian diseases (table S1) (*6*–*9*). We asked whether a small-molecule iron transporter could leverage transmembrane gradients of the labile iron pool (*2*) that selectively build up in such situations to restore the movement of iron into, within, and/or out of cells and thereby enable its use in endogenous iron-dependent physiological processes (Fig. 1A).

We specifically chose to study three disease-relevant iron-transporter deficiencies that disrupt iron movement in different directions, cellular locations, and tissues (*2*, *6*). Deficiencies of divalent metal transporter 1 (DMT1, also known as NRAMP2, DCT1, or SLC11A2) reduce apical iron uptake into duodenal enterocytes (fig. S1A) and prevent endosomal iron release in red blood cell progenitors (fig. S1B) (*2*, *6*). Mitoferrin (MFRN1, also known as SLC25A37) deficiencies in the inner mitochondrial membrane impair iron import into the mitochondrial matrix (fig. S1C) (*10*, *11*). Ferroportin (FPN1, also known as IREG1, MTP1, or SLC40A1) deficiencies reduce iron efflux from the gut epithelium (fig. S1D) and reticuloendothelial macrophages (fig. S1E) (*12*–*15*).

Previous reports suggest that high doses of hydrophilic iron chelators, such as deferiprone and pyridoxal isonicotinoyl hydrazone (PIH), as well as more lipophilic derivatives, such as salicylaldehyde isonicotinoyl hydrazone (SIH), may bind and relocate excess iron (*16*, *17*). However, the corresponding complexes of many of these chelators show limited membrane permeation and may require the action of colocalized proteins to achieve iron mobilization (*18*, *19*). We alternatively sought to identify a lipophilic small molecule that can autonomously perform transmembrane iron transport to promote physiology in cells and animals missing each of the aforementioned proteins.

Small molecule–mediated functional complementation in yeast

To find such a molecule, we designed a modified functional complementation experiment (*20*), in which candidate compounds known or predicted to bind iron were tested for their capacity to restore growth to a strain of *Saccharomyces cerevisiae* missing the iron-transporting complex FetFtr1 (fet3Δftr1Δ; fig. S1F) (*21*). Deferiprone, PIH, and SIH did not restore growth (fig. S2B). In contrast, the natural product hinokitiol (Hino, β-thujaplicin; Fig. 1B)—originally isolated by Nozoe from essential oil of the *Chamaecyparis taiwanensis* (Taiwan Hinoki) tree (*22*)—was highly effective (Fig. 1, C to E). This natural product has previously been characterized as a potent chelator of iron and other metals (*23*–*26*) that exerts a range of other biological activities (*25*–*31*). Hinokitiol restored growth to iron transporter–deficient yeast under fermentative and respiratory conditions (Fig. 1D and fig. S3A) and independently of known siderophore transporters (fig. S3B) (*21*, *32*). Hinokitiol sustainably restored growth to wild-type levels with similar doubling times (Fig. 1E and fig. S3, C to E).

Synthetic removal of the C2 oxygen atom by hydrogenolysis yielded C2-deoxy hinokitiol (C2deOHino; Fig. 1B and fig. S3F). In contrast to hinokitiol, C2deOHino cannot bind or transport iron and thus served as a negative control (fig. S4, A and B). Hinokitiol dose-dependently restored yeast growth, whereas C2deOHino did not (Fig. 1F). Hinokitiol, but not C2deOHino, also restored iron influx (Fig. 1G), and hinokitiol-mediated growth was iron-dependent (fig. S3, G and H). Growth restoration was similarly observed with other lipophilic α-hydroxy ketones, but not with hydrophilic α-hydroxy ketones or small molecules that transport other ions (fig. S2, A to C, and fig. S3I).

Characterization of iron binding and transport with hinokitiol

Biophysical experiments were performed to better understand the capacity for hinokitiol to bind and transport ferrous and ferric iron across lipid membranes. This natural product rapidly binds iron to form a hinokitiol:iron complex, as evidenced by

[1]Department of Chemistry, University of Illinois at Urbana-Champaign, Urbana, IL 61801, USA. [2]Department of Biochemistry, University of Illinois at Urbana-Champaign, Urbana, IL 61801, USA. [3]Division of Hematology, Department of Medicine, Brigham and Women's Hospital, Harvard Medical School, Boston, MA 02115, USA. [4]Department of Pharmaceutical Sciences, Northeastern University, Boston, MA 02115, USA. [5]Department of Nutritional Sciences, University of Michigan School of Public Health, Ann Arbor, MI 48109, USA. [6]Department of Genetic and Complex Diseases, Harvard T.H. Chan School of Public Health, Boston, MA 02115, USA. [7]Division of Hematology-Oncology, Department of Medicine, Boston Children's Hospital, Harvard Medical School, Boston, MA 02115, USA. [8]Department of Pediatric Oncology, Dana-Farber Cancer Institute, Harvard Medical School, Boston, MA 02215, USA. [9]Carle-Illinois College of Medicine, University of Illinois at Urbana-Champaign, Champaign, IL 61820, USA.
***Corresponding author. Email: wessling@hsph.harvard.edu (M.W.-R.); j.kim@neu.edu (J.K.); bpaw@rics.bwh.harvard.edu (B.H.P.); mdburke@illinois.edu (M.D.B.)**

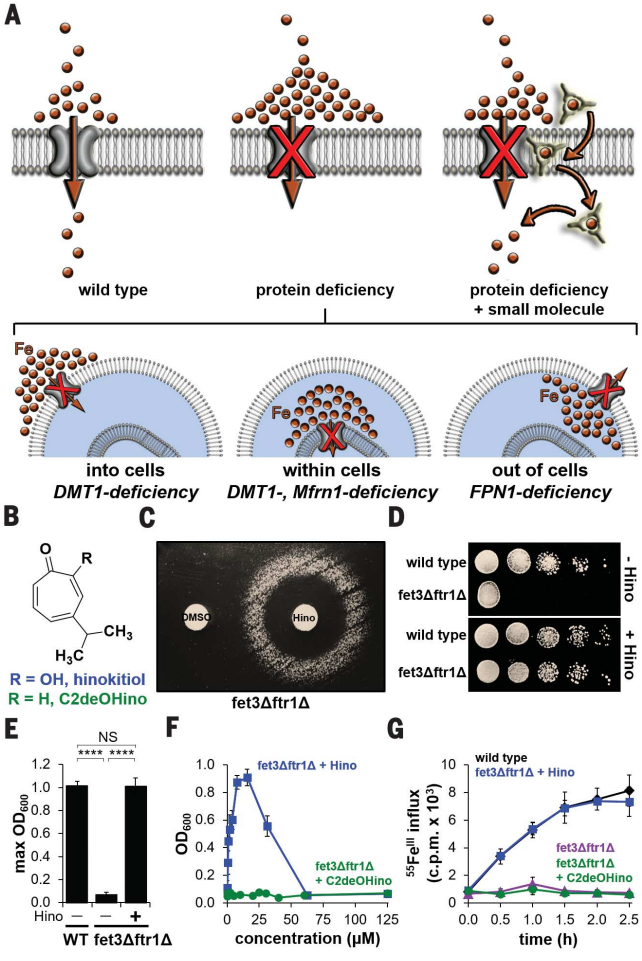

Fig. 1. Restoring physiology to iron transporter–deficient organisms. (**A**) A small molecule that autonomously performs transmembrane iron transport is hypothesized to harness local ion gradients of the labile iron pool that selectively accumulate in the setting of missing iron-transport proteins. Brown spheres represent labile iron, which includes both ionic iron and iron weakly bound to small molecules such as citrate. (**B**) Structures of the small molecule hinokitiol and the transport-inactive derivative C2-deoxy hinokitiol (C2deOHino). (**C**) Growth of fet3Δftr1Δ yeast cells streaked on a low-iron synthetic dextrose (SD) agar plate containing 10 μM $FeCl_3$ was restored by disc diffusion with hinokitiol (Hino) at intermediate concentrations. (**D**) In the absence of hinokitiol, reduced fet3Δftr1Δ yeast cell growth was observed on low-iron SD agar plates containing 10 μM $FeCl_3$ by serial 10-fold dilution plating [from OD_{600} (optical density at 600 nm) = 1.0]. Under identical conditions, but in the presence of 10 μM hinokitiol, restored cell growth was observed on the same low-iron SD agar plates. (**E**) Yeast cell growth in liquid SD media containing 10 μM $FeCl_3$ in the absence or presence of 10 μM hinokitiol (n = 3). NS, not significant; ****$P \leq 0.0001$. (**F**) Hinokitiol restored growth of fet3Δftr1Δ yeast, whereas C2deOHino did not (n = 3). (**G**) Hinokitiol increased ^{55}Fe influx into fet3Δftr1Δ yeast, whereas C2deOHino did not (n = 3). In (E) to (G), graphs depict means ± SEM. h, hours.

an immediate change in color and ultraviolet-visible (UV-vis) spectra upon addition of ferric or ferrous iron (Fig. 2, A and B, and fig. S4, A and C). Unlike water-soluble iron chelators (*17*), hinokitiol:iron complexes predominantly partition into nonpolar solvents rather than water (Fig. 2A and fig. S3I). For example, >95% of hinokitiol:iron complexes partition into octanol rather than water, whereas deferiprone:iron complexes exhibit >95% partitioning into water (fig. S3I). This is consistent with quantitative extraction of hinokitiol:iron complexes from the aqueous to the organic layer, as determined by inductively coupled plasma mass spectrometry (ICP-MS) analysis (fig. S4D).

Hinokitiol strongly binds ferrous and ferric iron, with an association constant (K_a) of 5.1×10^{15} for ferrous iron and 5.8×10^{25} for ferric iron, the latter of which is more than an order of magnitude stronger than that of deferiprone (fig. S4, E to H, and table S2). Consistent with its high affinity, hinokitiol removes iron from iron-citrate complexes that compose the labile iron pool (fig. S4A). In buffered solution, competition experiments indicate that hinokitiol can also remove iron from the iron-binding proteins transferrin and ferritin, but only when hinokitiol is used in >1000-fold excess relative to transferrin and >1,000,000-fold excess relative to ferritin (fig. S4, I to K). Hinokitiol has a pK_a of 7.33, suggesting that both the neutral and anionic states are accessible under physiological conditions (fig. S4L). Moreover, ^{56}Fe bound to hinokitiol readily exchanged with ^{55}Fe in solution, with >20% exchange observed within 10 min (fig. S4M). Thus, the binding of iron by hinokitiol under physiological conditions is expected to be highly dynamic, which may allow for the facile release of iron from hinokitiol complexes to iron-binding proteins and its subsequent use in iron-related physiological processes.

Hinokitiol autonomously transported both ferrous and ferric iron across model liposomal membranes, whereas C2deOHino, deferiprone, and PIH showed minimal transport (Fig. 2, C and D). Although the transport-active complex remains to be identified, speciation studies are consistent with the predominant formation of a 3:1 Hino:Fe^{III} complex in aqueous buffer (fig. S4, N and O). X-ray crystallography of tris(hinacolato) iron(III) revealed a pair of C_1-symmetric complexes, each composed of a lipophilic outer shell encasing a hydrophilic and iron-binding central core (Fig. 2E and fig. S4P).

Hinokitiol is a broad-spectrum metallophore capable of binding and transporting multiple divalent metals (fig. S5, A to I, and table S3). Hinokitiol competitively bound 10 times as much Cu^{II} as Fe^{II} and transported Cu^{II} 80 times as fast as Fe^{II} in liposomes, yet the low accessibility of copper likely leads to high iron selectivity in vivo. Specifically, the cytosolic labile copper pool is 10 orders of magnitude smaller than that of iron (table S3) (*33*–*35*). This is attributed to robust networks of transporters, chaperones, storage proteins, and regulators that bind Cu^{II} with exceptional affinities and selectivities (*35*). For example, the transcriptional activator Mac1, which is essential in regulating yeast copper homeostasis, binds copper with a dissociation constant (K_d) of 9.7×10^{-20} M (*35*). Upon treatment of fet3Δftr1Δ yeast with hinokitiol, intracellular iron levels increased relative to those in vehicle-treated controls, whereas levels of manganese, cobalt, nickel, zinc, and copper were unchanged (fig. S5J).

The redox potential of $Fe(Hino)_3$ in aqueous systems is estimated to be as low as –361 mV, compared with +770 mV for free iron (Fig. 2F; fig. S6, A to J; and tables S2, S4, and S6). Consistent with this, in a reducing environment, the reduction of iron(III) was slowed in the presence of hinokitiol, but it was still nearly quantitative in less than 2 hours (fig. S6, K and L). Moreover, the redox potential increased with decreasing pH and decreasing hinokitiol concentrations (fig. S6, F, I, and J, and tables S4 and S5). Collectively, these data suggest that both ferric and ferrous iron should be readily accessible in the presence of hinokitiol under physiological conditions.

Restored iron transport promotes absorption and hemoglobinization in cells

We thus asked whether hinokitiol could promote iron movement into, within, and/or out of mammalian cells deficient in DMT1, MFRN1, or FPN1. We first studied iron uptake and transepithelial transport in differentiated DMT1-deficient Caco-2 gut epithelia monolayers (fig. S1A) (*36*, *37*) established through stable short hairpin RNA (shRNA) transfection (fig. S7, A to C). Relative to wild-type controls, DMT1-deficient monolayers showed reduced iron uptake into cells and reduced transepithelial iron transport to the basolateral fluid after apical addition of $^{55}FeCl_3$ (Fig. 3, A and B). Apical addition of hinokitiol (500 nM) restored uptake and transport (Fig. 3, A and B) in a time frame commensurate with dwell times in the gut (Fig. 3C). Hinokitiol did not disrupt monolayer integrity (fig. S7D), caused no observable toxicity (table S7), and did not affect basal DMT1 expression (fig. S7, B and C). Hinokitiol-mediated transport occurred across a range of pHs found

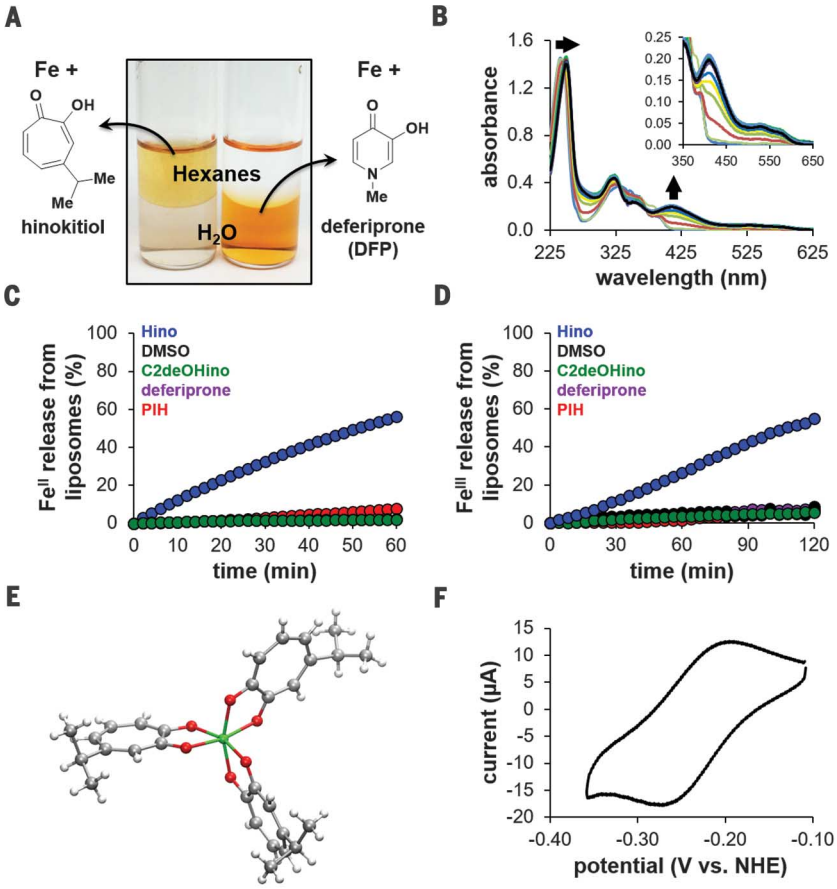

Fig. 2. Physical characteristics of hinokitiol binding and transport. (**A**) In contrast to water-soluble chelators, such as deferiprone, the hinokitiol-iron complex partitions into nonpolar solvents. (**B**) UV-vis titration study of hinokitiol with increasing $FeCl_3$ indicates that hinokitiol binds iron. Arrows indicate changes in the UV spectrum with increasing iron from 0:1 Fe:Hino (light blue line with least absorbance at 420 nm) to 6:1 Fe:Hino (black line). (**C** and **D**) In contrast to water-soluble iron chelators and C2deOHino, hinokitiol autonomously promotes the efflux of (C) ferrous and (D) ferric iron from model POPC liposomes (n = 3). (**E**) X-ray crystal structure of a C_1-symmetric $Fe(Hino)_3$ complex. (**F**) Cyclic voltammogram of the iron-hinokitiol complex in 0.1 M Tris buffer in 1:1 MeOH:H_2O at pH = 7.2, using 500 μM Hino and 100 μM $Fe(NO_3)_3$ with a 100 mV/s scan rate (NHE, normal hydrogen electrode). In (C) and (D), graphs depict representative runs of three independent experiments; in (F), a representative run of four independent experiments is shown.

throughout the duodenum and increased with decreasing pH (fig. S7E). Whereas hinokitiol promoted uptake and transport over a wide range of concentrations, C2deOHino and subtoxic concentrations of the iron chelators deferiprone, deferoxamine, PIH, and SIH did not promote both uptake and transport (fig. S7, F and G, and table S7). High concentrations of these more hydrophilic iron chelators instead decreased iron uptake into DMT1-deficient monolayers (fig. S7F).

If DMT1 is missing, depleted, or hypomorphic, intracellular iron(II) efflux from endosomes of erythroid precursors is precluded, thus preventing hemoglobinization (fig. S1B) (*2*, *6*, *38*). We tested for dimethyl sulfoxide (DMSO)–induced differentiation and hemoglobinization in DS19 murine erythroleukemia (MEL) cells (*39*) and shRNA-transfected DMT1-deficient MEL cells (fig. S8, A to C), in the absence or presence of hinokitiol. Control cells differentiated normally after 3 days, as indicated by the characteristic pink color of hemoglobin in cell pellets (Fig. 3D) and brown staining of hemoglobinized cells with *o*-dianisidine (fig. S8, D and E). Reduced hemoglobinization was observed in DMT1-deficient cells (Fig. 3, D to F, and fig. S8, D to F). Three days of hinokitiol treatment (1 μM) restored ^{55}Fe uptake (fig. S8F), ^{55}Fe incorporation into heme (Fig. 3F), and hemoglobinization (Fig. 3D and fig. S8, D to J) without observable toxicity (fig. S8K and table S7), whereas C2deOHino had no effect (Fig. 3, E and F, and fig. S8, F, I, and J). As expected, no differentiation was observed in the absence of DMSO, with or without hinokitiol treatment (fig. S8L).

Having observed hinokitiol-mediated transport of iron into and within DMT1-deficient cells, we asked whether the same small molecule could also substitute for other iron-transport proteins. MFRN1 in the inner mitochondrial membrane imports iron into the mitochondrial matrix for hemoglobinization (fig. S1C) (*2*, *10*). MFRN1-deficient MEL cells developed through CRISPR-Cas9–mediated knockout (fig. S9A) exhibited reduced hemoglobinization by *o*-dianisidine staining (Fig. 3G), ^{55}Fe uptake (fig. S9B), and ^{55}Fe incorporation into heme (fig. S9C) after DMSO induction. Hinokitiol (1 μM) restored hemoglobinization, whereas C2deOHino had no effect (Fig. 3G and fig. S9, B and C), suggesting hinokitiol-mediated mitochondrial delivery of iron. As expected, hinokitiol did not promote hemoglobinization to MEL cells that were instead deficient in a protein involved in porphyrin biosynthesis (TMEM14CΔ) (fig. S9, D to F).

FPN1 deficiencies reduce iron efflux across the basolateral membrane of gut epithelia (fig. S1D) and from reticuloendothelial macrophages (fig. S1E) that recycle iron from senescent erythrocytes (*13*, *14*). Quercetin (*40*) and hepcidin (*41*) were used to transiently decrease FPN1 levels in differentiated Caco-2 epithelia monolayers and J774 macrophages (*41*), respectively (fig. S9, G to J). Hinokitiol (1 μM) restored transepithelial iron transport in FPN1-deficient Caco-2 monolayers (Fig. 3H and fig. S9K) without affecting iron uptake (Fig. 3I) or disrupting monolayer integrity (fig. S9L). Hinokitiol also time- and dose-dependently restored iron release from FPN1-deficient J774 macrophages without observable toxicity (Fig. 3, J and K; fig. S9M; and table S7).

Site- and direction-selective buildup and release of iron gradients

We next probed the mechanistic hypothesis that hinokitiol promotes site- and direction-selective iron movement by harnessing built-up transmembrane iron gradients in transporter-deficient systems (Fig. 1A). We first visualized compartmentalized iron in DMT1-deficient MEL cells by using fluorescent dyes (fig. S10, A to C) (*42*, *43*). An OxyBURST Green–bovine serum albumin conjugate localized to endosomes fluoresces upon iron-mediated oxidation (fig. S10C), and fluorescence emissions from the turn-off probes calcein green (fig. S10A) and rhodamine B-[(1,10-phenanthrolin-5-yl)-aminocarbonyl]benzyl ester (RPA) (fig. S10B) in the cytosol and mitochondria, respectively, are quenched upon iron binding. Relatively low endosomal, high cytosolic, and high mitochondrial iron levels were observed in DMSO-induced control MEL cells (Fig. 4A and fig. S11, A, B, E, and H). We observed twofold increases in iron-promoted OxyBURST Green fluorescence in DMT1-deficient MEL cells (Fig. 4A and fig. S11, A and B), along with reduced cytosolic and mitochondrial iron (Fig. 4A and fig. S11, A, E, and H). Hinokitiol treatment decreased OxyBURST Green fluorescence 2.1-fold and concomitantly quenched calcein green and RPA fluorescence (Fig. 4A and fig. S11, A to J). These data support hinokitiol-mediated release of built-up pools of endosomal iron into the cytosol and subsequent mitochondrial uptake.

Calcein green and ^{55}Fe studies also revealed a buildup of labile iron in FPN1-deficient J774 macrophages relative to wild-type cells (Fig. 4, B to D). Hinokitiol direction-selectively promoted both iron influx to (Fig. 4E) and efflux

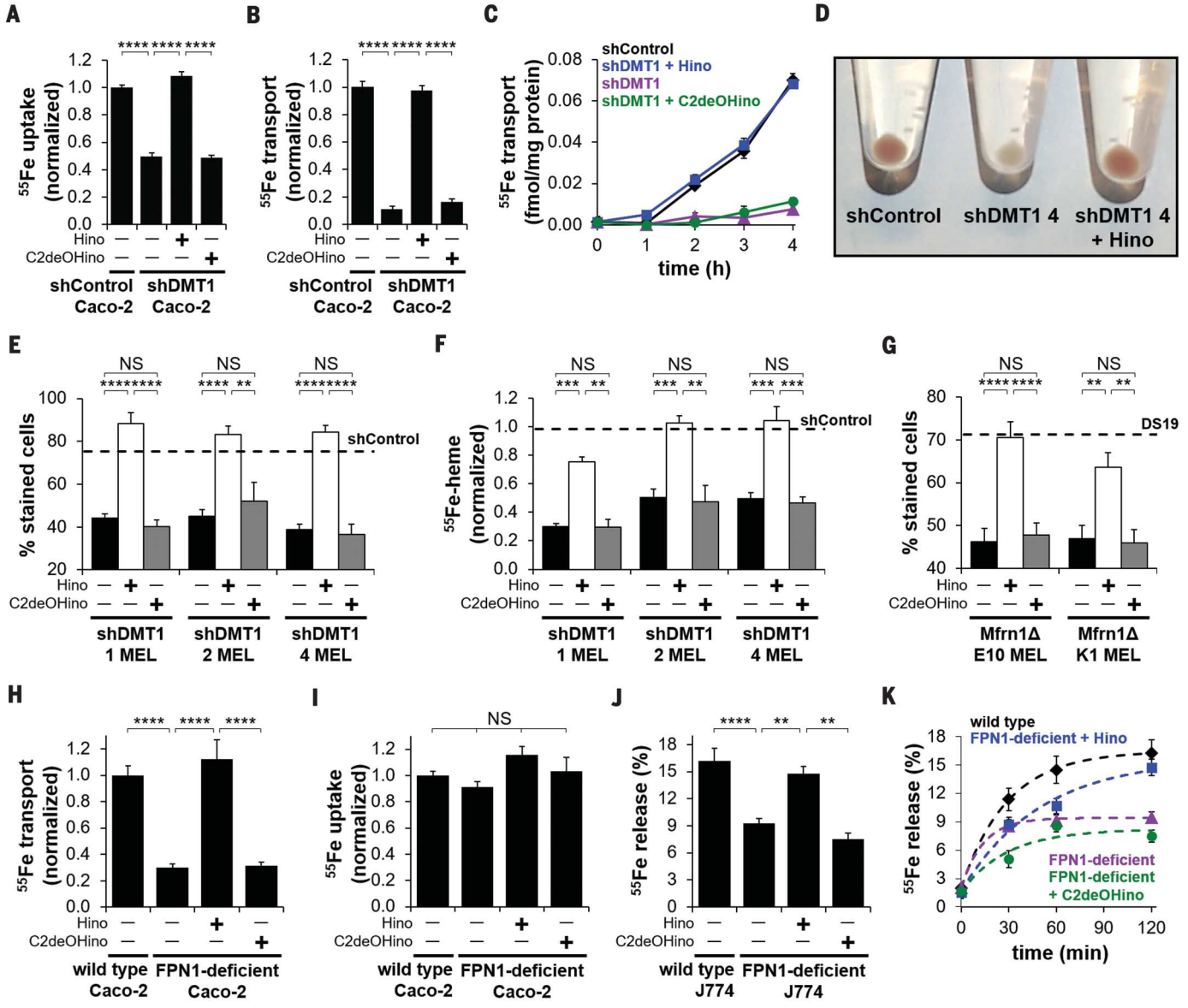

Fig. 3. Hinokitiol restores mammalian cell physiology. (**A**) ^{55}Fe uptake into DMT1-deficient (shDMT1) Caco-2 monolayers and (**B**) transepithelial transport (apical to basolateral) indicated that hinokitiol (500 nM) restored normal iron absorption (n = 3). shControl refers to Caco-2 monolayers that were transfected with a nontargeting control shRNA plasmid. (**C**) Hinokitiol-promoted ^{55}Fe transport occurs on time scales commensurate with dwell times in the gut (n = 3). (**D**) Cell pellets from shControl and hinokitiol-treated (1 μM) DMT1-deficient MEL cells appear pink, characteristic of hemoglobin, whereas DMT1-deficient cell pellets do not. (**E**) ImageJ quantification of MEL cells stained brown with o-dianisidine (n = 6 to 48). The dashed line represents shControl levels. (**F**) ^{55}Fe incorporation into heme in hinokitiol-rescued DMT1-deficient MEL cells (n = 3 to 23). The dashed line represents shControl levels. (**G**) Hinokitiol increases the number of o-dianisidine–stained MFRN1-deficient MEL cells (n = 21 to 48). The dashed line represents DS19 (wild-type) levels. (**H**) Hinokitiol (1 μM) restores ^{55}Fe transepithelial transport across FPN1-deficient Caco-2 monolayers (**I**) without affecting iron uptake (n = 12). (**J**) Hinokitiol (5 μM) promotes the release of ^{55}Fe from hepcidin-treated FPN1-deficient J774 macrophages (t = 2 hours; n = 6 to 20). (**K**) Time-dependent release of ^{55}Fe from wild-type J774 macrophages and FPN1-deficient J774 macrophages treated with DMSO, hinokitiol, or C2deOHino (n = 6 to 20). In (A) to (C), and (E) to (K), graphs depict means ± SEM. NS, not significant; $^{**}P \le 0.01$; $^{***}P \le 0.001$; $^{****}P \le 0.0001$.

from (Fig. 3J and fig. S9M) J774 macrophages, depending on the presence of high extracellular or intracellular iron, respectively. Further, hinokitiol-mediated iron(II) and iron(III) efflux from liposomes and iron(III) uptake into J774 macrophages was directly proportional to the transmembrane iron gradients (Fig. 4, E to G, and fig. S12, A to D). Last, we loaded iron into J774 macrophages, rinsed the cells to remove extracellular iron, and stained them with calcein green (fig. S12E). Hinokitiol addition [at time (t) = 5 min] rapidly increased calcein green fluorescence, whereas vehicle and C2deOHino had no effect (Fig. 4, H and I; fig. S13, A to C; and movie S1). We then reversed the gradient in these same cells by external addition of $FeCl_3$ (t = 12 min) (fig. S12E). DMSO or C2deOHino treatment of cells had no effect (Fig. 4I and fig. S13, A and C), whereas quenching of calcein green fluorescence was observed with hinokitiol treatment (Fig. 4, H and I; fig. S13B; and movie S1). These results are consistent with initial hinokitiol-mediated release of iron from J774 macrophages when intracellular iron levels are high, followed by hinokitiol-mediated uptake of iron into these macrophages when this transmembrane gradient is reversed by addition of extracellular iron (fig. S12E).

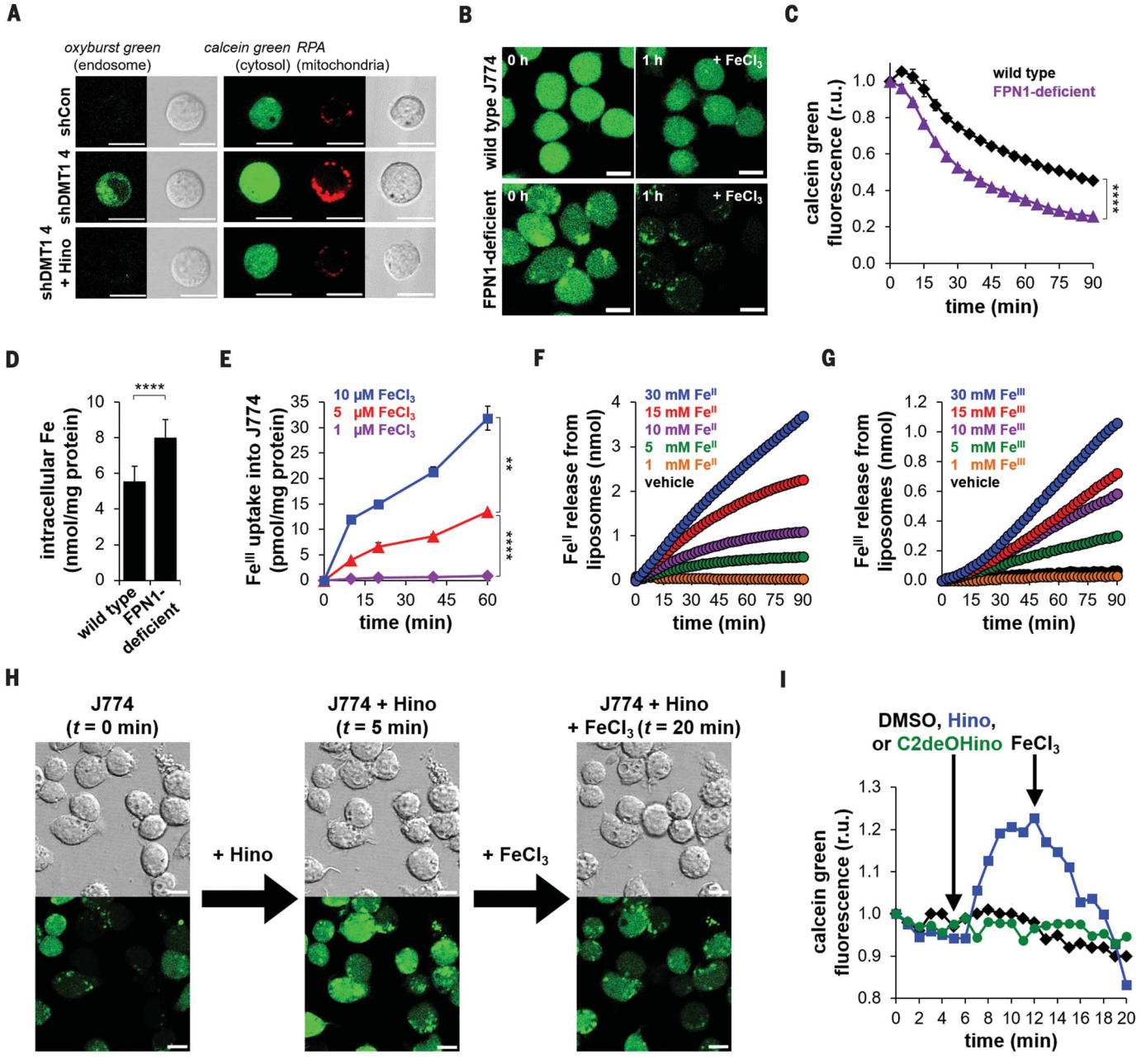

Fig. 4. Hinokitiol leverages built-up iron gradients. (**A**) Representative fluorescence images of differentiated shControl and DMT1-deficient MEL cells in the absence or presence of hinokitiol (1 μM), using OxyBURST Green, calcein green, and RPA to detect relative endosomal, cytosolic, and mitochondrial iron levels, respectively. A buildup of labile iron was observed in endosomes of DMT1-deficient cells, which was released after hinokitiol treatment. (**B** and **C**) A buildup of intracellular labile iron was observed in FPN1-deficient J774 macrophages treated with 200 μM $FeSO_4$ by quenching of calcein green fluorescence ($n = 3$). (**D**) Iron(III) uptake into J774 macrophages treated with 50 μM $FeCl_3$ similarly revealed a buildup of total intracellular iron in FPN1-deficient cells after 4 hours, as observed using ^{55}Fe as a radiotracer ($n = 8$). (**E**) Increased extracellular iron(III) levels increased rates of iron uptake into J774 macrophages treated with hinokitiol (1 μM), as observed using ^{55}Fe as a radiotracer ($n = 3$). (**F** and **G**) Increased intraliposomal (F) ferrous and (G) ferric iron led to increased rates of iron efflux in the presence of hinokitiol (10 μM) ($n = 3$). No efflux was observed in the absence of hinokitiol. (**H**) Fluorescence imaging of cytosolic iron with calcein green, using artificially created iron gradients in opposite directions in J774 macrophages. Cells were loaded with $FeSO_4$ (200 μM) and rinsed; then, hinokitiol (100 μM) was added at $t = 5$ min. An increase in fluorescence was observed, consistent with decreased intracellular labile iron. The gradient was then reversed in these same cells by addition of 100 μM $FeCl_3$ to the media at $t = 12$ min. Fluorescence quenching was observed, consistent with iron uptake. (**I**) Representative ImageJ quantification of calcein green fluorescence in iron-loaded J774 cells with addition of DMSO, hinokitiol, or C2deOHino at $t = 5$ min and $FeCl_3$ at $t = 12$ min. Scale bars, 10 μm in (A) and 20 μm in (B) and (H). In (C) to (E), graphs depict means ± SEM; $^{**}P \le 0.01$; $^{****}P \le 0.0001$. In (F) and (G), graphs depict means of three independent experiments. In (I), a representative graph from six independent experiments is shown. r.u., relative units.

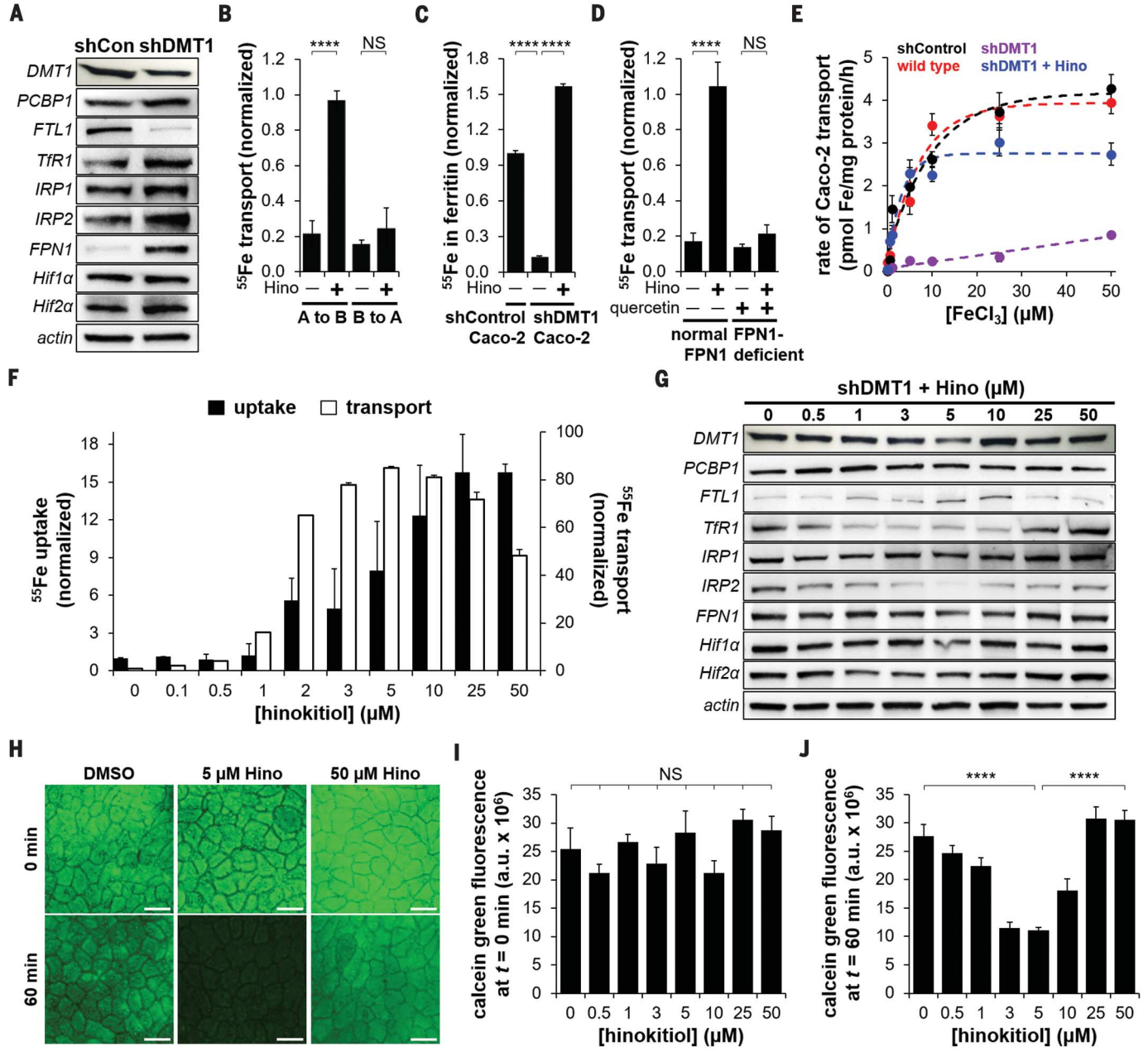

Fig. 5. The endogenous network is involved in hinokitiol-mediated Caco-2 transport. (**A**) Representative Western blot images of proteins involved in iron absorption and regulation indicate an anemic state in shDMT1 Caco-2 monolayers to promote maximal iron absorption. (**B**) Unidirectional hinokitiol-mediated transport in shDMT1 Caco-2 monolayers observed with apical or basolateral addition of hinokitiol (500 nM) and ^{55}Fe radiotracer (n = 3). (**C**) Determination of ^{55}Fe levels in immunoprecipitated ferritin in Caco-2 monolayers (n = 3). (**D**) Knockdown of FPN1 in shDMT1 Caco-2 monolayers with quercetin abrogates hinokitiol-mediated transport (n = 3). (**E**) Rates of Caco-2 transport with varying concentrations of iron 4 hours after treatment with DMSO or hinokitiol (500 nM) (n = 3). The rates of transport level off with increasing iron concentrations. (**F**) Increased doses of hinokitiol increase uptake into shDMT1 Caco-2 monolayers apically treated with 25 μM $FeCl_3$; however, a bimodal effect is observed in transepithelial iron transport at 5 μM hinokitiol (n = 3). (**G**) Representative Western blot images of proteins involved in iron absorption and regulation after treatment with increasing hinokitiol and 25 μM $FeCl_3$. Bimodal effects were similarly observed in protein levels involved in iron absorption and regulation. (**H**) Intermediate concentrations of hinokitiol lead to significant calcein green quenching in shDMT1 monolayers treated with 25 μM $FeCl_3$ after 1 hour, consistent with increased labile iron. This effect was reversed at high doses of hinokitiol. Scale bar, 20 μM. (**I** and **J**) ImageJ quantification of calcein green fluorescence in these monolayers (n = 3 to 6). In (B) to (F), (I), and (J), graphs depict means ± SEM; NS, not significant; ****$P \leq 0.0001$.

Mechanisms for maintaining iron homeostasis

We then asked whether endogenous networks of other ion-transport proteins and regulators (*2*) in iron transporter–deficient cells can collaborate with the small molecule hinokitiol to help promote restoration of site- and direction-selective iron transport while still maintaining iron homeostasis. In yeast, the intracellular movement and storage of iron is dependent on a proton gradient known as the proton motive force, which is generated by the adenosine triphosphate (ATP)–dependent active ion-transport proteins Pma1 and V-ATPase in the plasma and vacuolar membranes, respectively (*21*, *35*). Consistent with the

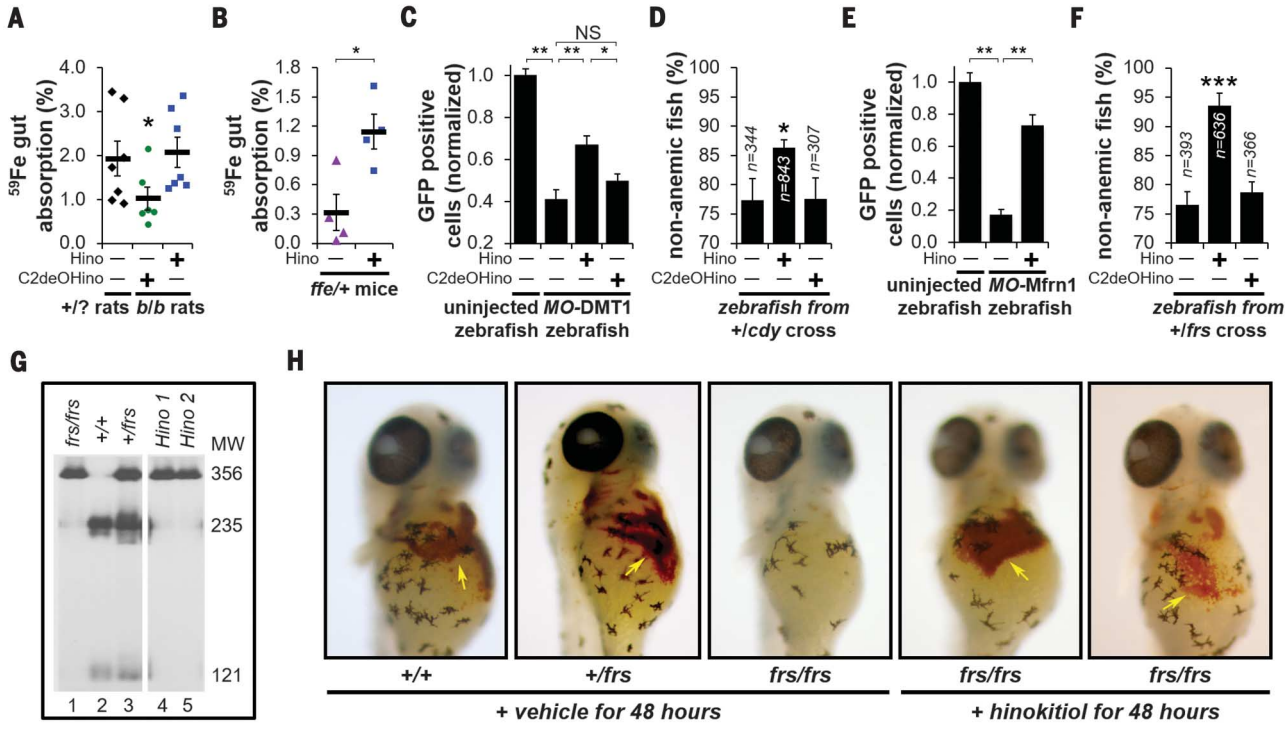

Fig. 6. Hinokitiol restores physiology in iron transporter–deficient animals. (**A** and **B**) Oral gavage of 1.5 mg/kg hinokitiol promotes the gut absorption of ^{59}Fe into (A) DMT1-deficient Belgrade (*b/b*) rats and (B) FPN1-deficient flatiron (*ffe/+*) mice after 1 hour (n = 4 to 7). (**C**) Hinokitiol treatment (1 μM) added to the embryo media (containing 10 μM iron citrate) at 24 hpf and incubation for an additional 48 hours increases the number of GFP-positive erythroids (detected by FACS analysis) in Dmt1-deficient morphant zebrafish from a line of transgenic fish containing GFP-tagged erythroids (n = 7 to 17). (**D**) Hinokitiol decreases the number of anemic fish from a heterozygous cross of *+/cdy* fish, as determined by *o*-dianisidine staining, whereas C2deOHino does not. (**E**) Hinokitiol (1 μM) increases the number of GFP-positive erythrocytes in Mfrn1-deficient morphant zebrafish (n = 3 to 13). (**F**) Hinokitiol increases the number of nonanemic embryos from a heterozygous cross of *+/frs* fish. (**G**) Embryos from a heterozygous cross of *+/frs* fish were genotyped by restriction enzyme digestion with BsrI restriction enzyme. Lanes 4 and 5 correspond to *frs/frs* fish treated with hinokitiol for 48 hours. (**H**) Hinokitiol-treated *frs/frs* fish stain brown with *o*-dianisidine, whereas anemic *frs/frs* fish do not, indicating increased hemoglobin levels after hinokitiol treatment. Graphs depict means ± SEM in (A) to (C) and (E) and weighted means ± SEM in (D) and (F); NS, not significant; *$P \le 0.05$; **$P \le 0.01$; ***$P \le 0.001$.

dependence of hinokitiol-mediated iron transport on this proton motive force, hinokitiol-rescued fet3Δftr1Δ yeast were exceptionally sensitive to chemical inhibition of Pma1 and V-ATPase, but not to off-pathway inhibitors (fig. S14, A to C).

In intestinal epithelia, iron-transport proteins are transcriptionally and translationally regulated to maintain systemic iron levels while avoiding overload (*2*, *44*). Specifically, levels of the apical H^+/Fe^{2+} symporter DMT1, heavy (FTH1) and light (FTL1) chains of ferritin responsible for sequestering excess iron, basolateral efflux protein FPN1, and transferrin receptor 1 (TFR1) are translationally regulated through short hairpin iron response elements (IREs) located at the 5′ and 3′ untranslated regions of the corresponding mRNA transcripts (fig. S15A) (*2*). Iron-sensing iron response proteins (IRP1 and IRP2) bind to these IREs to block translation (5′-IRE, *FTH1*, *FTL1*, *FPN1*) or stabilize mRNA (3′-IRE, *DMT1*, *TFR1*) under iron starvation (fig. S15A). Upon iron stimulation and binding, IRPs dissociate from the mRNAs, reversing their described effects. Transcriptional regulation is achieved through the transcriptional activator hypoxia-inducible factor 2α (HIF2α), which is degraded after O_2- and iron-mediated proline hydroxylation (fig. S15B) (*2*). HIF2α activates transcription of *FPN1* to evade IRE-mediated translational repression under iron deprivation (*2*).

Consistent with these homeostatic mechanisms, an anemic state (*45*) was initially observed in DMT1-deficient Caco-2 monolayers, with decreased levels of ferritin and increased levels of FPN1 (Fig. 5A and fig. S14, D to L), thus providing a favorable cellular environment for small molecule–mediated iron transport. Providing support for functional collaboration with these endogenous proteins, hinokitiol-mediated iron uptake and transport across DMT1-deficient Caco-2 monolayers was unidirectional (Fig. 5B and fig. S14M). Apical treatment with this low dose of hinokitiol (500 nM) allowed for ^{55}Fe incorporation into ferritin (Fig. 5C), possibly mediated by the high-affinity iron chaperone poly(rC)-binding protein 1 (PCBP1) (*2*). Last, quercetin-mediated knockdown of FPN1 (*40*) antagonized hinokitiol-mediated transmembrane transport without affecting apical uptake (Fig. 5D and fig. S14, N to P).

Moreover, increased rates of transepithelial transport in DMT1-deficient monolayers were observed with increased concentrations of apical $FeCl_3$, but these effects leveled off at higher concentrations of iron (Fig. 5E). Further, a similar leveling of transmembrane transport was observed when the same monolayers were treated with a persistent iron gradient (25 μM $FeCl_3$) and increasing concentrations of hinokitiol (Fig. 5F). This phenomenon was evident over a wide range of hinokitiol and iron concentrations (fig. S16). We thus asked how the endogenous system responds to the hinokitiol-mediated changes in cellular iron status in the presence of a persistent iron gradient. Consistent with IRP-mediated translational regulation, decreased IRP2, increased ferritin subunits (5′-IREs), and decreased TFR1 (3′-IRE) protein levels were observed as a function of hinokitiol concentrations up to 5 μM in the presence of a persistent iron gradient (Fig. 5G and fig. S17, A to E). The transcription factors HIF1α and HIF2α similarly decreased along with decreased *FPN1* mRNA and FPN1 protein levels (Fig. 5G and fig. S17, F to I). As expected, IRE-independent expression of the cytosolic iron chaperone PCBP1 and HIF2α-independent *FTH1* mRNA levels did not change, and no changes in FPN1 were observed upon the addition of hinokitiol in the absence of iron (Fig. 5G and

fig. S17, K to N). A modest reversal of these effects was observed with higher concentrations of hinokitiol (Fig. 5G and fig. S17, A to J). Visualization of cytosolic iron with calcein green indicated that incubation of DMT1-deficient Caco-2 monolayers with increasing hinokitiol led to increased labile iron up to 5 μM (Fig. 5, H to J). Further increases in hinokitiol prevented fluorescence quenching, possibly because of competitive intracellular chelation of labile iron at high doses of this strongly binding metallophore (Fig. 5, H to J). These results collectively support the conclusion that the endogenous homeostatic networks can collaborate with the small molecule hinokitiol to help promote iron transport while maintaining its homeostasis and preventing ferritoxicity.

On the basis of this mechanistic framework, we hypothesized that hinokitiol would have relatively minimal effects in wild-type cells. We tested the capacity for the same concentrations of hinokitiol to perturb transepithelial iron transport, hemoglobinization, and iron release in normal Caco-2 monolayers, MEL cells, and J774 cells, respectively (fig. S18, A to F). In contrast to the hinokitiol-promoted increases in transepithelial iron transport (Fig. 3B), hemoglobinization (Fig. 3G), and iron release (Fig. 3J) observed in the corresponding protein-deficient systems, negligible effects were observed in hinokitiol-treated wild-type systems under identical conditions (fig. S18, A to F). Collectively, these results are consistent with hinokitiol restoring site- and direction-selective iron transport by harnessing gradients that selectively build up across lipid membranes missing specific iron-transport proteins.

Restored gut iron absorption and peripheral hemoglobinization in animals

We were thus encouraged to ask whether hinokitiol could restore gut iron absorption and hemoglobinization in animal models of these iron-transporter deficiencies. DMT1 and FPN1 deficiencies in duodenal enterocytes reduce rates of iron absorption in the gut by disrupting apical iron uptake into cells and basolateral efflux into the blood, respectively (*2*, *6*, *12*–*15*). We tested gut iron absorption in DMT1-deficient Belgrade (*b/b*) rats (*6*) and FPN1-deficient flatiron (*ffe/+*) mice (*14*, *15*) upon administration of a single dose of ^{59}Fe and 1.5 mg of hinokitiol per kilogram of body weight via oral gavage. Higher doses of hinokitiol are reported to be nontoxic in rats subjected to chronic oral administration for 2 years (*46*). Similar to the reduced iron absorption previously reported in *b/b* rats (*47*), a twofold reduction in ^{59}Fe absorption was observed in C2deOHino-treated *b/b* rats relative to sibling controls (*+/+* or *+/b*) (Fig. 6A and fig. S19A). Treatment of *b/b* rats with hinokitiol increased ^{59}Fe absorption back to control levels after 1 hour (Fig. 6A and fig. S19A). Consistent with our previous results (*15*), *ffe/+* mice also absorbed iron at low rates (Fig. 6B). Hinokitiol increased ^{59}Fe absorption in *ffe/+* mice after 1 and 2 hours (Fig. 6B and fig. S19B). A statistically significant increase in the rate of ^{59}Fe absorption was observed in hinokitiol-treated wild-type mice after 1 hour, but not after 2 hours (fig. S19C).

We have previously shown restoration of hemoglobinization in Mfrn1-deficient zebrafish through ectopic expression of Mfrn1 protein with complementary RNA (*10*). *Danio rerio* is well established as a powerful model organism in the study of hematopoiesis (*48*), and we used it to test whether chronic treatment with a small-molecule iron transporter could restore hemoglobinization in Dmt1 and Mfrn1 deficiencies (*10*, *49*). We first performed morpholino-mediated transient knockdown of Dmt1 in a *Tg(globinLCR:eGFP)* zebrafish strain expressing green fluorescent protein (GFP)–tagged erythrocytes (*50*). Injection of a designed antisense morpholino targeting the exon 4–intron 4 junction of premature *dmt1* mRNA reduced steady-state *dmt1* levels (fig. S19D) and decreased the number of GFP-positive erythroid cells detected by fluorescence-activated cell sorting (FACS) analysis (Fig. 6C). Addition of hinokitiol to the embryo media 24 hours postfertilization (hpf) and incubation for an additional 2 days promoted hemoglobinization in these DMT1-deficient morphant zebrafish without observable toxicity, whereas C2deOHino had no effect (Fig. 6C). We further tested whether hinokitiol could similarly restore hemoglobinization in genetically mutated *chardonnay* (*cdy*^{te216}) zebrafish, which contain a nonsense mutation leading to truncated Dmt1 and thereby exhibit severe hypochromic, microcytic anemia (*49*). A heterozygous cross of *+/cdy* fish led to a Mendelian distribution of ~75% healthy (*+/+* and *+/cdy*) and ~25% anemic (*cdy/cdy*) embryos in each clutch after *o*-dianisidine staining 72 hpf (Fig. 6D). Hinokitiol treatment for 2 days increased the number of fish exhibiting high hemoglobin levels, whereas C2deOHino had no effect (Fig. 6D).

We also tested hemoglobinization in Mfrn1-deficient morphant *Tg(globinLCR:eGFP)* zebrafish (*10*, *50*). Forty-eight hours of hinokitiol treatment restored hemoglobinization and the number of GFP-positive erythrocytes in these morphants (Fig. 6E). Last, we tested whether hinokitiol could restore hemoglobinization in genetically mutated *frascati* (*frs*^{tq223}) zebrafish, which contain a missense mutation leading to an inactive Mfrn1 mitochondrial protein and profound anemia during embryogenesis (*10*, *11*). Hinokitiol treatment of embryos collected from a heterozygous cross of *+/frs* fish prevented the anemic phenotype (Fig. 6F). Genotyped (Fig. 6G) healthy larvae (*+/+* and *+/frs*) exhibited brown staining with *o*-dianisidine, whereas untreated *frs/frs* fish did not (Fig. 6H). Hinokitiol treatment restored brown staining to *frs/frs* fish (Fig. 6H). As expected, hinokitiol did not affect *sauternes* (*sau*^{tb223}) zebrafish (*51*) deficient in the initial enzyme involved in porphyrin biosynthesis (Alas2) (fig. S19E), indicating the specificity of hinokitiol effects to defects in iron transport.

Outlook

We found that a small molecule, hinokitiol, can restore site- and direction-selective iron transport in different cells deficient in three distinct iron-transport proteins, and the same compound can promote dietary gut iron absorption or peripheral hemoglobinization in corresponding animal models. Mechanistic studies support the role of transmembrane ion gradients that build up in the setting of missing iron transporters, enabling hinokitiol to restore site- and direction-selective transmembrane iron transport. Further, endogenous protein-based homeostatic mechanisms interface with this small molecule to promote iron-related physiological processes without disrupting other cellular processes.

Like hinokitiol, many ion-transport proteins are imperfectly selective. However, the relative abundance of different ions contributes to increased selectivity in living systems. For example, protein chloride channels are largely unselective with respect to chloride versus bromide and iodide, but the low natural abundance of the latter halogens favors chloride selectivity in vivo (*1*, *52*). Differential ion accessibility further enhances the in vivo selectivity observed for many imperfect ion-transport proteins (*33*–*35*). Like hinokitiol, DMT1 and FPN1 transport Co^{2+}, Mn^{2+}, Zn^{2+}, and/or Cu^{2+} (*6*, *13*, *15*). However, high-affinity metalloproteins markedly decrease the labile pool of these other metals, leading to higher accessibility and thus selective binding and transport of iron in vivo (*33*–*35*).

These findings provide a conceptual framework and proof-of-concept demonstration to support the pursuit of small-molecule surrogates for missing or dysfunctional iron-transport proteins that underlie many human diseases. It has recently been recognized that acquired deficiencies of FPN1 underlie the anemia of chronic inflammation that frequently occurs in patients suffering from a number of common diseases, including rheumatoid arthritis, systemic lupus erythematosus, and inflammatory bowel disease (*9*). Further, this approach may have potential in promoting the rapid excretion of excess iron that builds up in tissues (e.g., liver or brain) in many diverse iron-overload disorders.

These results also reveal frontier opportunities to probe biology by using small molecules that autonomously perform protein-like functions. For example, our results demonstrate that in both cells and zebrafish, hinokitiol-mediated rescue of physiology distinguishes between defects in porphyrin biosynthesis and iron transport, which can be challenging to differentiate using genetic and biochemical techniques. Because networks of active and passive ion-transport proteins similarly underlie the directional movement of many other ions in most living systems, including humans, our findings may also have even broader scientific and therapeutic implications.

REFERENCES AND NOTES

1. E. Gouaux, R. Mackinnon, *Science* **310**, 1461–1465 (2005).
2. M. W. Hentze, M. U. Muckenthaler, B. Galy, C. Camaschella, *Cell* **142**, 24–38 (2010).
3. V. S. Shah *et al.*, *Science* **351**, 503–507 (2016).
4. F. Yi *et al.*, *Science* **352**, aaf2669 (2016).
5. P. Imbrici *et al.*, *Front. Pharmacol.* **7**, 121 (2016).
6. N. C. Andrews, *Nat. Rev. Genet.* **1**, 208–217 (2000).
7. N. C. Andrews, *N. Engl. J. Med.* **341**, 1986–1995 (1999).
8. P. T. Lieu, M. Heiskala, P. A. Peterson, Y. Yang, *Mol. Aspects Med.* **22**, 1–87 (2001).

9. G. Weiss, L. T. Goodnough, *N. Engl. J. Med.* **352**, 1011–1023 (2005).
10. G. C. Shaw *et al.*, *Nature* **440**, 96–100 (2006).
11. J. Chung *et al.*, *J. Biol. Chem.* **289**, 7835–7843 (2014).
12. A. Donovan *et al.*, *Nature* **403**, 776–781 (2000).
13. A. T. McKie *et al.*, *Mol. Cell* **5**, 299–309 (2000).
14. I. E. Zohn *et al.*, *Blood* **109**, 4174–4180 (2007).
15. Y. A. Seo, M. Wessling-Resnick, *FASEB J.* **29**, 2726–2733 (2015).
16. Y. S. Sohn, W. Breuer, A. Munnich, Z. I. Cabantchik, *Blood* **111**, 1690–1699 (2008).
17. H. C. Hatcher, R. N. Singh, F. M. Torti, S. V. Torti, *Future Med. Chem.* **1**, 1643–1670 (2009).
18. X. P. Huang, M. Spino, J. J. Thiessen, *Pharm. Res.* **23**, 280–290 (2006).
19. J. L. Buss, M. Hermes-Lima, P. Ponka, *Adv. Exp. Med. Biol.* **509**, 205–229 (2002).
20. A. G. Cioffi, J. Hou, A. S. Grillo, K. A. Diaz, M. D. Burke, *J. Am. Chem. Soc.* **137**, 10096–10099 (2015).
21. M. R. Bleackley, R. T. A. Macgillivray, *Biometals* **24**, 785–809 (2011).
22. T. Nozoe, *Bull. Chem. Soc. Jpn.* **11**, 295–298 (1936).
23. B. E. Bryant, W. C. Fernelius, *J. Am. Chem. Soc.* **76**, 1696–1697 (1954).
24. M. C. Barret, M. F. Mahon, K. C. Molloy, J. W. Steed, P. Wright, *Inorg. Chem.* **40**, 4384–4388 (2001).
25. K. Nomiya *et al.*, *J. Inorg. Biochem.* **98**, 46–60 (2004).
26. K. Nomiya *et al.*, *Inorg. Chim. Acta* **362**, 43–55 (2009).
27. C. Meck, M. P. D'Erasmo, D. R. Hirsch, R. P. Murelli, *MedChemComm* **5**, 842–852 (2014).
28. Y. Ido *et al.*, *Cell Prolif.* **32**, 63–73 (1999).
29. K. Murakami, Y. Ohara, M. Haneda, R. Tsubouchi, M. Yoshino, *Basic Clin. Pharmacol. Toxicol.* **97**, 392–394 (2005).
30. M. J. Lee, J. W. Kim, E. G. Yang, *Biochem. Biophys. Res. Commun.* **396**, 370–375 (2010).
31. G. Böhme, P. Schönfeld, U. Küster, W. Kunz, H. Lyr, *Acta Biol. Med. Ger.* **39**, 1153–1163 (1980).
32. G. Ghssein *et al.*, *Science* **352**, 1105–1109 (2016).
33. L. A. Finney, T. V. O'Halloran, *Science* **300**, 931–936 (2003).
34. L. A. Ba, M. Doering, T. Burkholz, C. Jacob, *Metallomics* **1**, 292–311 (2009).
35. M. S. Cyert, C. C. Philpott, *Genetics* **193**, 677–713 (2013).
36. A. Espinoza *et al.*, *Biol. Trace Elem. Res.* **146**, 281–286 (2012).
37. I. Hubatsch, E. G. E. Ragnarsson, P. Artursson, *Nat. Protoc.* **2**, 2111–2119 (2007).
38. M. Tabuchi, T. Yoshimori, K. Yamaguchi, T. Yoshida, F. Kishi, *J. Biol. Chem.* **275**, 22220–22228 (2000).
39. C. Friend, W. Scher, J. G. Holland, T. Sato, *Proc. Natl. Acad. Sci. U.S.A.* **68**, 378–382 (1971).
40. M. Lesjak *et al.*, *PLOS ONE* **9**, e102900 (2014).
41. M. D. Knutson, M. Oukka, L. M. Koss, F. Aydemir, M. Wessling-Resnick, *Proc. Natl. Acad. Sci. U.S.A.* **102**, 1324–1328 (2005).
42. B. P. Espósito, W. Breuer, Z. I. Cabantchik, *Biochem. Soc. Trans.* **30**, 729–732 (2002).
43. Y. S. Sohn *et al.*, *Haematologica* **97**, 670–678 (2012).
44. M. Arredondo, A. Orellana, M. A. Gárate, M. T. Núñez, *Am. J. Physiol.* **273**, G275–G280 (1997).
45. D. L. Zhang, R. M. Hughes, H. Ollivierre-Wilson, M. C. Ghosh, T. A. Rouault, *Cell Metab.* **9**, 461–473 (2009).
46. N. Imai *et al.*, *J. Toxicol. Sci.* **31**, 357–370 (2006).
47. T. Veuthey, M. Wessling-Resnick, *Front. Pharmacol.* **5**, 82 (2014).
48. S. Avagyan, L. I. Zon, *Hum. Gene Ther.* **27**, 287–294 (2016).
49. A. Donovan *et al.*, *Blood* **100**, 4655–4659 (2002).
50. J. J. Ganis *et al.*, *Dev. Biol.* **366**, 185–194 (2012).
51. A. Brownlie *et al.*, *Nat. Genet.* **20**, 244–250 (1998).
52. C. Miller, *Nature* **440**, 484–489 (2006).

ACKNOWLEDGMENTS

We gratefully acknowledge A. Ringel for assistance with zebrafish experiments and A. Li for assistance with octanol/water partition coefficients. We thank J. Hou, K. Muraglia, and R. Chorghade for independently repeating the results shown in Fig. 1C; fig. S2, A to C; Fig. 3, A and B; and fig. S9M. We further acknowledge D. Kosman and C. Philpott for providing yeast strains, L. Zon for the *Tg(globinLCR:eGFP)* transgenic zebrafish line, W. Boulanger for the generous gift of comenic acid, and J. Katzenellenbogen for use of a liquid scintillation counter. We thank M. Garrick, L. Garrick, and M. Fleming for helpful discussions. We thank D. Gray and the George L. Clark X-Ray Facility for x-ray analysis, M. Sivaguru and the Carl R. Woese Institute for Genomic Biology for assistance with confocal microscopy, B. Pilas and the Roy J. Carver Biotechnology Center for help with flow cytometry, and the University of Illinois School of Chemical Sciences microanalysis facility for ICP-MS and optical emission spectrometry. Support was provided by NIH through grants GM118185 (to M.D.B.), K01 DK106156 and F32 DK098866 (to Y.Y.Y.), R01 DK070838 and P01 HL032262 (to B.H.P.), K99ES024340 (to Y.A.S.), R01ES0146380 and R01DK064750 (to M.W.-R.), and R21EB023025 (to J.K.). M.D.B. also thanks the Howard Hughes Medical Institute (HHMI) for funding. A.S.G. was a NSF Graduate Fellow. J.B.A. was supported by the HHMI Exceptional Research Opportunities Program. M.D.B. and A.S.G. are inventors on patent application 62/101,706, submitted by the University of Illinois at Urbana-Champaign, which covers the use of small-molecule iron transporters to treat deficiencies of iron-transport proteins. Additional data reported in this paper are available in the supplementary materials. Crystallographic data for $Fe(Hino)_3$ are available free of charge from the Cambridge Crystallographic Data Centre under reference CCDC 1536565.

SUPPLEMENTARY MATERIALS

www.sciencemag.org/content/356/6338/608/suppl/DC1
Materials and Methods
Supplementary Text
Figs. S1 to S31
Tables S1 to S8
References (*53–109*)
Movie S1

20 June 2016; resubmitted 30 November 2016
Accepted 21 March 2017
10.1126/science.aah3862

Restored iron transport by a small molecule promotes absorption and hemoglobinization in animals

Anthony S. Grillo, Anna M. SantaMaria, Martin D. Kafina, Alexander G. Cioffi, Nicholas C. Huston, Murui Han, Young Ah Seo, Yvette Y. Yien, Christopher Nardone, Archita V. Menon, James Fan, Dillon C. Svoboda, Jacob B. Anderson, John D. Hong, Bruno G. Nicolau, Kiran Subedi, Andrew A. Gewirth, Marianne Wessling-Resnick, Jonghan Kim, Barry H. Paw and Martin D. Burke

Science **356** (6338), 608-616.
DOI: 10.1126/science.aah3862

Shipping iron around in small packages

Iron plays a crucial role in a wide variety of biological functions, which in turn rely on the proteins that transport the metal in and out of cells. Grillo *et al.* used a simple lipophilic small molecule that binds iron ions to restore transport in animal models with deficiencies in iron transporters. This cyclic ketol, hinokitiol, was first tested in yeast and then shown to promote gut iron absorption in rats and mice, as well as hemoglobin production in zebrafish.

Science, this issue p. 608